Cell Tissue Res (1993) 274:567–577

Cell & Tissue Research

Ultrastructural location of calcium and magnesium during mineralisation of the cuticle of the shore crab, as determined by the K-pyroantimonate method and X-ray microanalysis

Philippe Compère[1], John A. Morgan[2], Gerhard Goffinet[3]

[1] Laboratory of Animal Morphology, University of Liège, 22, Quai Ed. van Beneden, B-4020 Liège, Belgium
[2] School of Pure and Applied Biology, University of Wales College of Cardiff, P.O. Box 915, Cardiff CF1 3TL, UK
[3] Laboratory of General Biology, University of Liège, 22, Quai Ed. van Beneden, B-4020 Liège, Belgium

Received: 9 September 1992 / Accepted: 16 April 1993

Abstract. We have investigated the distribution of Ca^{2+} and Mg^{2+} in the new cuticle of moulting shore crabs (*Carcinus maenas*), using the K-pyroantimonate method in combination with X-ray microanalysis in order to identify antimony precipitates. During the premoult period, Ca^{2+} and Mg^{2+} accumulate in well-defined sites of the new pigmented layer. After moulting, mineralisation appears to begin preferentially at these sites. These form a honeycomb-like structure that quickly increases the rigidity of the new cuticle, with a small recruitment of material from extraneous sources. Mineralisation of the principal layer, on the other hand, immediately follows deposition of the organic matrix. Our experiments also provide evidence that the epidermal cell extensions associated with the pore canals are the means by which Ca^{2+} and Mg^{2+} are transferred from the epidermis into the mineralising cuticular layers. The plasma membrane of these cell extensions appears densely lined by particles of antimony precipitate that probably mark the location of the transporting sites. Shortly after moulting, the distribution of mineral deposits is such that the cell extensions cross the mineralised lamellae of the principal layer and constitute preferential access routes to the pigmented layer, where mineralisation is still in progress.

Key words: Cuticle – Mineralisation – Calcium, magnesium, location – Pyroantimonate – X-ray microanalysis – *Carcinus maenas* (Crustacea, Decapoda)

Introduction

The crab cuticle is an organic-mineral protective exoskeleton of particular interest because it undergoes cyclic moulting processes. From a structural standpoint (for a review, see Cameron 1985), it consists of a thin superficial epicuticle (for a detailed description, see Compère and Goffinet 1992) and a thick lamellate procuticle including three layers: the pigmented layer, the principal layer and the membranous layer (according to the terminology of Drach 1939). The organic matrix of the procuticle is mainly composed of horizontal chitin-protein microfibres exhibiting a twisted plywood arrangement (Bouligand 1965, 1972). This architecture is disturbed by two main vertical elements: the interprismatic septa and the pore canals. The interprismatic septa, which delimit prismatic spaces, are polygonal imprints left in the pigmented layer by the margins of the epidermal cells (Vitzou 1882; Drach 1939; Giraud-Guille 1984a). The pore canals constitute a ramified system of tubules left by long epidermal cell extensions during moulting (Green and Neff 1972; Compère and Goffinet 1987a,b). In the hard cuticular regions or sclerites, the pigmented and principal layers are hardened by the presence of mineral deposits (Neville 1975; Roer and Dillaman 1984). In the cuticle of *Carcinus maenas*, mineral salts mostly consisting of Ca-Mg carbonates represent about 85% of the cuticular dry weight (Welinder 1975).

During the moult, crabs shedding their rigid mineralised exoskeleton are vulnerable until their new cuticle stiffens. Roer's data (1980) demonstrate high Ca deposition rates ($8–9 \times 10^{-8}$ mole/cm^2) in cuticular fragments of newly moulted *C. maenas* (stages A_1 and A_2). These results corroborate those of Vigh and Dendinger (1982) showing a rapid in vivo increase in the Ca content of the cuticle of the blue crab (*Callinectes sapidus*) until 10 days postmoult when the cuticle has achieved its rigidity. According to Drach (1937, 1939), Bouligand (1970) and Giraud-Guille and Quintana (1982), mineralisation begins only a few hours after ecdysis and follows successive steps. The calcite deposits first appear as spherulitic crystals all along the outer lamella of the pigmented layer (according to the previous authors) or inside the epicuticle (Travis 1957; Neville 1975; Roer and Dillaman 1984). Mineral deposition then progresses along the interprismatic septa and finally fills the free prismatic spaces. In the principal layer, mineralisation occurs simultaneously with the deposition of the lamellae and starts before the

Correspondence to: P. Compère

complete calcification of the pigmented layer. Several pathways have been proposed by authors to explain the transport of Ca and Mg into the cuticular layers, but all are hypothetical and the presence of mineral concretions inside the epicuticle remains questionable. Travis (1957, 1963, 1965), Travis and Friberg (1963) and Yano (1980) have observed calcite crystals in the lumen of pore canals and have hypothesised that these canals are involved in the cuticular transport of Ca. This interpretation has however largely been contested by Bouligand (1970) and Neville (1975). The experiments of Roer (1980) and Cameron (1989) have shown that the apical plasma membrane of epidermal cells takes part in a massive transport of Ca ions, probably effected by a Ca^{2+}ATPase and/or exchange mechanisms. Roer (1980) further regards the epidermal cell extensions associated with the intracuticular pore canals as a possible means for increasing the surface of the ion-transporting apical plasma membrane. This idea is also supported by Compère and Goffinet (1987b) who have proposed that the postmoult regression of the cell extensions is related to the progress of mineralisation. Yet there is no clear evidence to support the view that the cell extensions associated with the pore canals play a role in the mineralisation process. Many questions arise regarding how and when mineral ions reach the preferential mineralisation sites in the pigmented layer and, how they pass through the fully mineralised lamellae of the principal layer to be deposited in the prismatic spaces of the pigmented layer.

The aim of the present study was to determine the ultrastructural location and the path of Ca and Mg ions in the mineralising crab cuticle before and after ecdysis. To this end, the K-pyroantimonate cytochemical method was used in combination with X-ray microanalysis.

Materials and methods

Atlantic shore crabs (*Carcinus maenas* L.) were collected at the Marine Station of Wimereux (France). Fragments of the branchiostegite integument were excised from small animals (2–3 cm wide). Late premoult stages D_2-D_3 and the early postmoult stage A_2 (24 h postmoult) were determined according to the method of Drach and Tchernigovtzeff (1967).

K-pyroantimonate method

Preparation of a K-pyroantimonate stock solution. Just before use, a saturated solution was prepared as recommended by Appleton and Morris (1979). K-hexahydroxyantimonate [$KSb(OH)_6$; Aldrich, n°24, 728–6] was added to twice distilled water in the proportion of about 4% weight/volume. Gentle boiling was required for the almost complete dissolution of the salt. After cooling to room temperature, this solution was microfiltered on a Sartorius 0.45 µm filter and added to an equal volume of fixative solution.

Specimen treatment. Specimens were first fixed by immersion for 4 h at 20°C in a K-phosphate-buffered (0.1 M, pH 9.0) solution containing approximately 2% K-pyroantimonate and 2.5% glutaraldehyde. Osmolarity was adjusted to 700 mOsm with sucrose. After rinsing in the same buffer with K-pyroantimonate, samples were postfixed for 1 h at 20°C in buffered 1% osmium tetroxide also containing K-pyroantimonate, and were briefly rinsed in K-pyroantimonate-free buffer. To avoid any redissolution or displacement of the precipitate, specimens were not rinsed with distilled water but were directly dehydrated in an ethanol series and in propylene oxide (Mentré et al. 1986).

After being embedded in Epon 812, the samples were thin-sectioned with a diamond knife using a Sorvall Porter-Blum MT IIB ultramicrotome. They were then contrasted with uranyl acetate (Watson 1958) and lead citrate (Reynolds 1963). Formvar-coated grids were used to support sections of non-decalcified fragments from postmoulting crabs. Sections were examined in a Siemens 101 or a JEOL 100 SX electron microscope at an accelerating voltage of 80 kV.

Control experiments. Ethylene diamine tetraacetic acid (EDTA) (Titriplex III, Merck), a well-known chelating agent for divalent cations, was used both to avoid the precipitation reaction of Ca and Mg with pyroantimonate and to remove these salts from ultra-thin sections of embedded material. In the pre-embedding method, fragments were first briefly fixed (30 min–1 h at 20°C) in a buffered solution containing glutaraldehyde without K-pyroantimonate. They were then incubated for 4 h in 0.2 M EDTA, pH 8.0; the solution was renewed at hourly intervals. After a brief rinse in buffer, they were subjected to the general K-pyroantimonate procedure. In the postembedding method, ultra-thin sections were incubated for 1 h at 60°C in 0.2 M EDTA, pH 8.0. In order to remove non-specific K-pyroantimonate precipitates from the sections, grids were incubated in twice distilled water for 1 h at 60°C.

X-ray microanalysis. X-ray microanalysis was used to identify the precipitates in K-pyroantimonate-treated samples and directly to locate Ca and Mg in tissues. For this purpose, samples were prepared for freeze-substitution and freeze-sectioning.

Preparation of material. Tegumental fragments were fixed by direct immersion in liquid nitrogen with no cryoprotectant pretreatment. For freeze-substitution, they were progressively dehydrated in 10% 2,2-dimethoxypropane in acetone at temperatures increasing gradually from −70°C to −40°C over 5 days. The samples were impregnated overnight with Lowicryl HM20 resin at −40°C in the presence of silicagel. They were then transferred to pure resin in polyethylene Beem capsules. The samples were then allowed to polymerise under UV light for 2 days at −40°C and for 3 days at room temperature.

Preparation of the sections. Dry glass knives and an LKB ultramicrotome were used to produce semi-thin sections (0.5–1 µm thick) from Epon-embedded and Lowicryl HM20 freeze-substituted fragments. The glass knives were made just before use by means of an LKB knife-maker. Sections were then mounted on Formvar-coated titanium grids.

Semi-thin frozen sections were made with glass knives on a Sorvall Porter-Blum MT I ultramicrotome in a freezing-chamber at −100°C. Sections mounted on Formvar-coated titanium grids were dehydrated by ice sublimation in the vacuum chamber of a Balzers sputtering unit (type SCD 030). They were gradually warmed to room temperature and coated with a carbon film (15 nm).

X-ray microanalyser system. The transmission electronic analytical system used was a Philips EM 300, fitted with an EDAX energy-dispersive (solid-state) retractable spectrometer and an EDAX 707 B multichannel analyser. The analyser was interfaced with an EDIT mini-computer pre-programmed to perform "background subtract" functions (EDAX International Inc.). Details of the data processing treatment have been described previously by Morgan et al.(1975) and Morgan and Davies (1982).

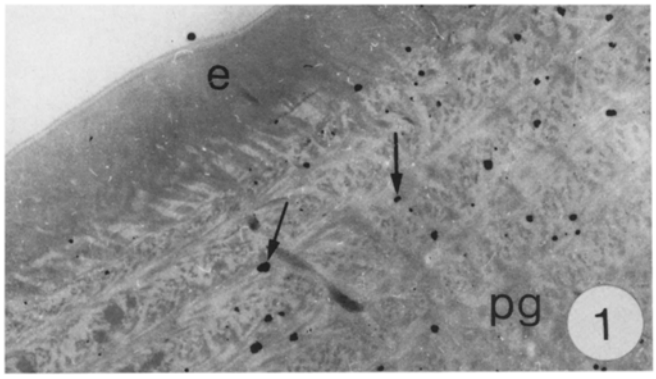

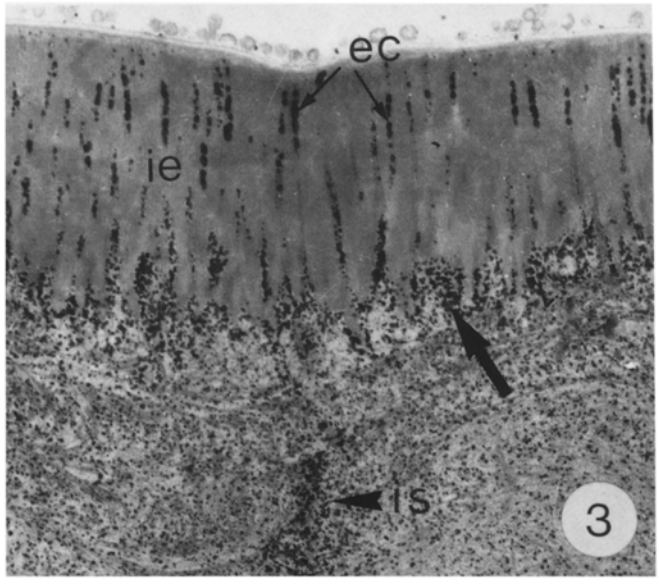

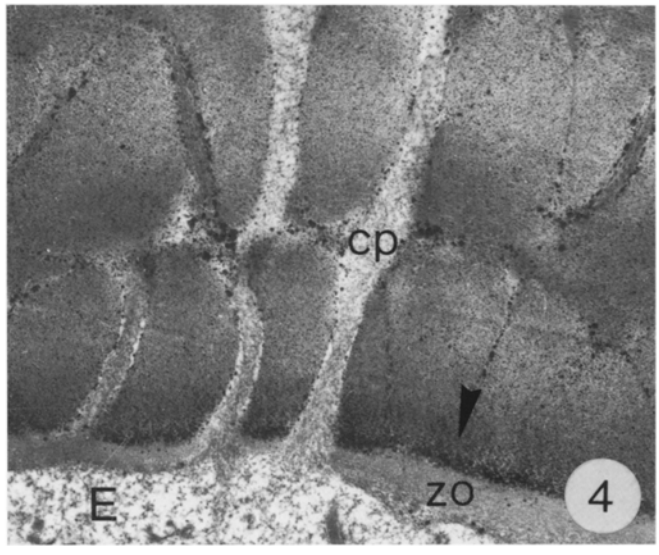

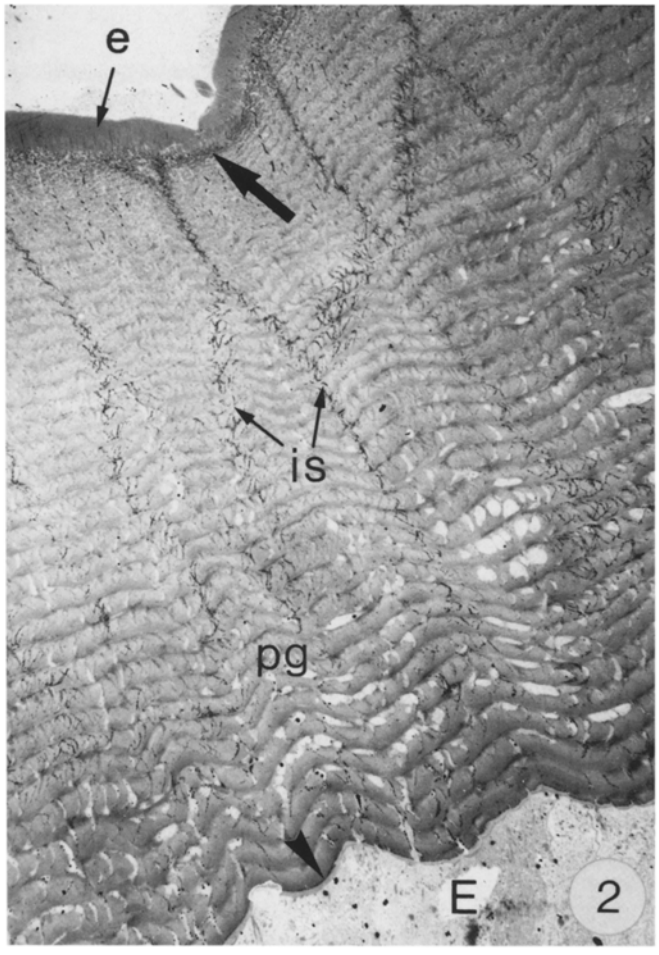

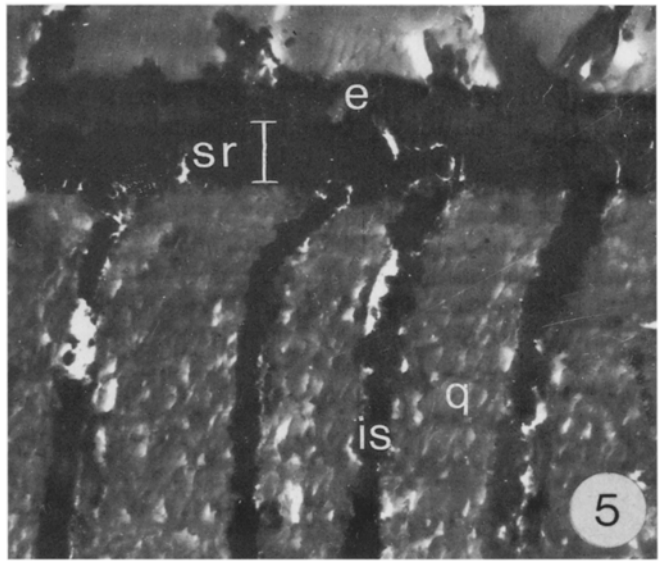

Fig. 1. Vertical section through the outer branchiostegite cuticle at stage A_2 showing randomly distributed coarse precipitate particles (*arrows*) following EDTA decalcification and fixation in K-pyroantimonate-containing solutions. *e* Epicuticle; *pg* pigmented layer. ×9000

Figs. 2–4. Vertical sections through the late premoult cuticle after incubation in K-pyroantimonate-containing fixative solutions. Fine precipitate particles are randomly scattered throughout the pigmented layer (*pg*) and accumulate at the level of three preferential sites: the subepicuticular region (*large arrows*), the interprismatic septa (*is*) and the base of the last deposited lamella (*arrowheads*)

Fig. 2. General view of the cuticle. *E* Epidermis; *e* epicuticle. ×2500

Fig. 3. Detail of the epicuticle and the upper part of the pigmented layer. *ec* Epicuticular canals; *ie* inner epicuticle; *oe* outer epicuticular layers. ×15000

Fig. 4. Detail of the lower lamellae of the pigmented layer crossed by epidermal cell extensions (*cp*). *E* Epidermis; *zo* organisation zone of the chitin-protein fibres. ×15000

Fig. 5. Vertical dry-cut semi-thin section from a freeze-substituted sample of the outer branchiostegite cuticle 24 h after exuviation (stage A_2). Mineral deposits appear highly electron-dense. *e* Epicuticle; *is* interprismatic septa; *q* prismatic spaces; *sr* subepicuticular region. ×4000

Results

Ultrastructural location of antimonate precipitates

All the sections of K-pyroantimonate-treated samples exhibited two kinds of electron-dense deposits, differing in particle size, location and solubility in water and EDTA. A coarse precipitate (particle diameter >100 nm) appeared randomly in the epidermis, in the haemolymph sinuses and in underlying connective-tissue cells. Inside the cells, it was uniformly distributed in the nucleus, cytoplasm and various organelles. It was never observed in the cuticle except in samples previously decalcified with EDTA (Fig. 1). Although the coarse precipitate was soluble in distilled water, it was not removed from the sections by 0.2 M EDTA at pH 8.0. A finer precipitate (particle diameter <100 nm) was mainly observed in the cuticle. Its formation was completely prevented by prior chelation of divalent cations (EDTA treatment). This fine precipitate was largely removed from the sections by EDTA, but not by distilled water. Moreover, its distribution in the cuticle varied according to the moulting stage.

At the late premoult stage (end of stage D_2), a fine granular electron-opaque deposit was scattered throughout the new pigmented layer (Fig. 2). There were three regions, however, that appeared as preferential precipitation sites where particles were closely packed, coalescing into large particles: the first lamella below the epicuticle, the interprismatic septa (Figs. 2, 3) and the last lamella above the epidermis (Figs. 2, 4). One narrow zone (0.6 μm in thickness) remained free of precipitate: a region of newly-deposited fibres separating the last lamella from the epidermis (Figs. 2, 4). The epicuticle, including the surface coat, the cuticulin layer and the inner epicuticle matrix, likewise remained devoid of dense deposit, except for epicuticular canals that contained some particles (Fig. 3). At this stage, the precipitate was seldom found associated with the pore canal cell extensions (Fig. 4).

By 24 h after ecdysis (stage A_2), mineralisation occurred in the pigmented layer and in the newly deposited principal layer. In the former, mineral successively appeared in the uppermost lamella, the interprismatic septa and the innermost lamella. In the latter, all lamellae became mineralised shortly after their deposition. Dry-cut semi-thin sections revealed mineral deposits appearing as electron-dense concretions (Fig. 5). In sections collected on water, most of these concretions were lost (Fig. 6). Under these conditions, mineralised sites appeared as electron-lucent areas. As during the pre-moulting stage, a fine scattering of minute particles filled the prismatic spaces of the pigmented layer that were not yet mineralised, whereas the regions that underlay the mineral deposits of the subepicuticular region and the principal layer (Fig. 9) exhibited a more intense, dense precipitate. At these levels, precipitates showed an unusual aspect, appearing as rings around electron-lucent spots corresponding to the newly deposited mineral. The size of these spots increased towards the fully mineralised regions.

A major dense precipitate was also associated with the plasma membrane of the pore canal cell extensions that crossed the fully mineralised lamellae of the principal layer (Figs. 6, 9) and that extended into the pigmented layer (Figs. 7, 8). Specifically, precipitate particles were located on the inner leaflet of the plasma membrane. They exhibited round or crescent-shaped sections, the largest diameter of which ranged from 30 to 60 nm (Fig. 9). Precipitate particles were lacking on the apical epidermal plasma membrane between cell extensions and within the cytoplasm of the epidermal cells.

X-ray microanalysis

The analysis of X-ray spectra (Fig. 10) of electron-dense precipitates obtained after K-pyroantimonate treatment revealed that Sb, K and Ca are the main elements composing the precipitates. Whereas the Sb peaks ($L_{\alpha 1}$ at 3.604 keV, $L_{\beta 1}$ at 3.843 keV and $L_{\beta 2}$ at 4.100 keV) were equally apparent on spectra of both coarse and fine precipitates, the two types of precipitate exhibited noticeably different compositions with respect to other elements. The spectrum of the coarse precipitate shows a major K peak ($K_{\alpha 1,2}$ at 3.310 keV), which the spectrum of the fine precipitate lacks. In contrast, a minor Mg peak ($K_{\alpha 1,2}$ at 1.253 keV) appears on the spectra of the fine precipitate (Figs. 10, 12) but is completely lacking on the spectra of the coarse precipitate. Ca peaks cannot at first glance be discerned, because the Ca $K_{\alpha 1,2}$ peak at 3.690 keV is too close to, and overlaps with, the Sb $L_{\alpha 1}$ peak at 3.604 keV. Differences between presumed Sb peaks only appear after careful scrutiny or if the spectra of the two precipitates are superimposed (Fig. 12). The spectrum from the coarse precipitate showed a peak at exactly 3.604 keV, corresponding to pure Sb, whereas the corresponding peak of the fine precipitate is slightly shifted towards higher energies (top at 3.650 keV), and exhibits obvious shouldering at 3.690 keV. We interpret the shift and shouldering as evidence of the presence of Ca in this precipitate. Similar peak shapes were obtained by analysing Ca-pyroantimonate precipitate from a standard $Ca(NO_3)_2/2Sb_2O_3 + 4KOH$ solution where the Sb/Ca ratio was 4:1 (Fig. 11). The overlapped Ca $K_{\alpha 1,2}$ peak could be revealed by stripping the Sb $L_{\alpha 1}$, $L_{\beta 1}$ and $L_{\beta 2}$ peaks from the spectra. Sb peaks suitable for subtraction were produced by analysing a Ca-free standard K-pyroantimonate (Fig. 13). In order to produce Sb peaks equal to those of the original spectrum, the two spectra were adjusted to the same scale using the antimony $L_{\beta 1}$ as reference, as it

Fig. 6. General view of a vertical ultra-thin section on a Formvar-coated grid. As a consequence of the loss of mineral deposits during floating on water, the mineralised zones appear electron-lucent. The mineralising region of the prismatic spaces is located below the epicuticle (*asterisk*). *cp* Epidermal cell extensions; *e* epicuticle; *is* interprismatic septa; *pg* pigmented layer; *pr* principal layer; *q* prismatic spaces; *sr* subepicuticular region. × 2200

Figs. 7–8. Vertical floated semi-thin (**7**) and ultra-thin (**8**) sections of the postmoult mineralising cuticle (stage A_2) after fixation in K-pyroantimonate-containing solutions. The pore canal cell extensions

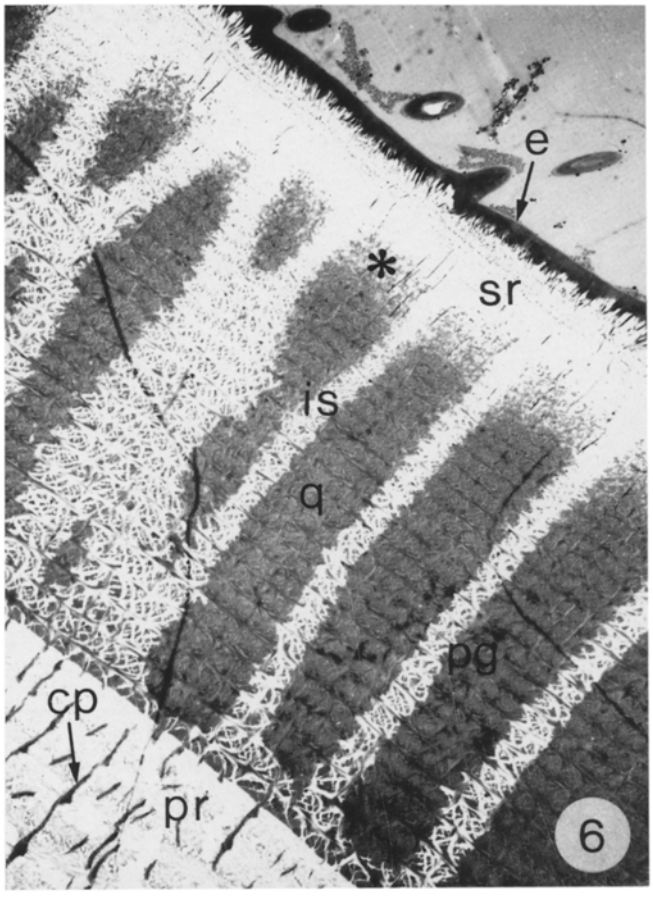

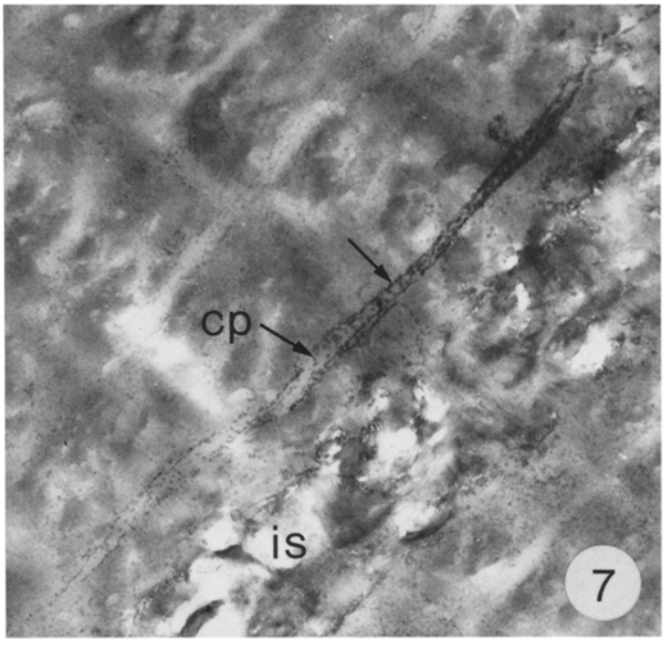

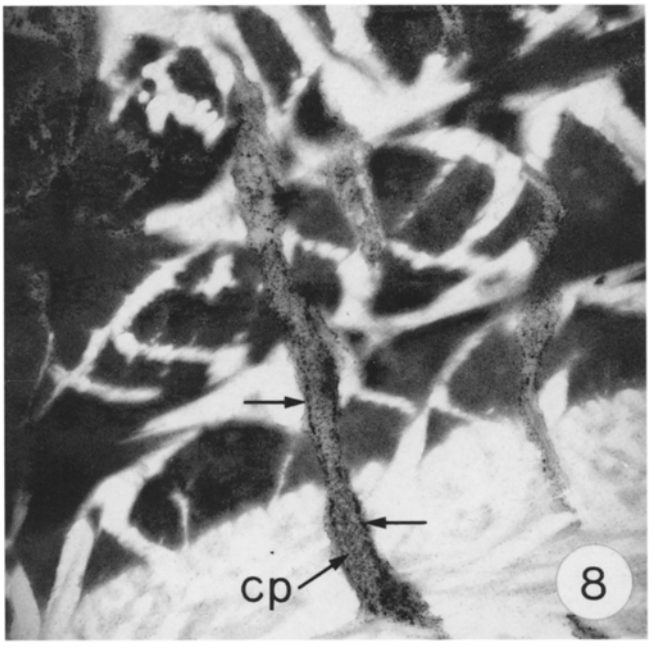

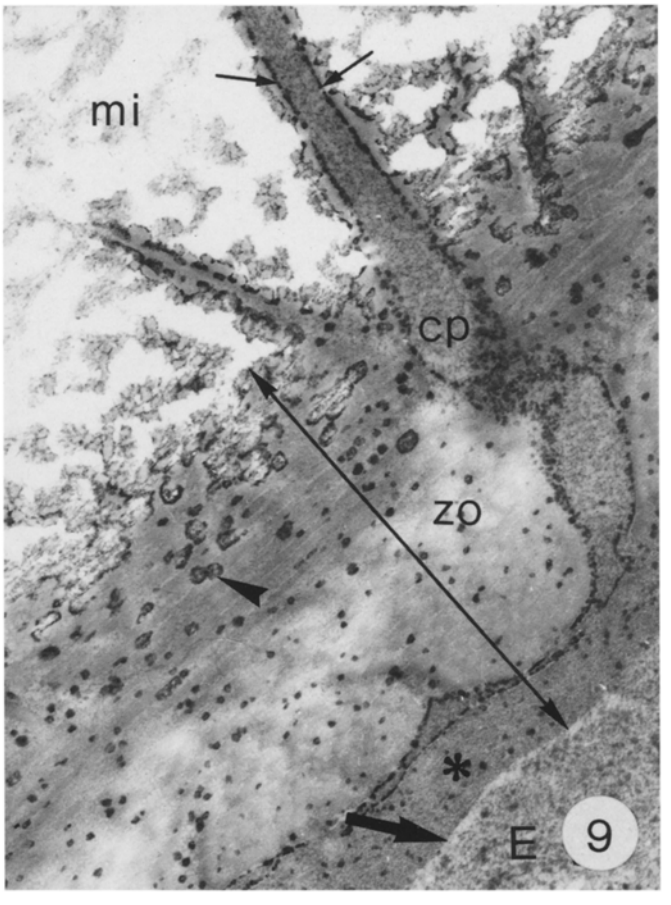

(*cp*) show abundant dense precipitate particles (*arrows*) associated with the inner leaflet of the plasma membrane

Fig. 7. Middle part of the pigmented layer. *is* Mineralised interprismatic septa. ×12000

Fig. 8. Limit between the pigmented layer and the principal layer. ×12000

Fig. 9. High magnification of a pore-canal-cell extension (*cp*) showing the lowest lamella of the principal layer 24 h postmoult (stage A_2) after fixation in K-pyroantimonate-containing solutions. Abundant dense precipitate particles (*arrows*) are associated with the inner leaflet of the plasma membrane. A dense precipitate also appears as rings around electron-lucent spots corresponding to newly deposited mineral (*arrowhead*). Precipitate particles are poorly represented in the most proximal part (*asterisk*) and are completely lacking along the epidermal cell plasma membrane (*large arrow*). *E* Epidermis; *mi* fully-mineralised zone; *zo* newly deposited cuticular zone where mineralisation occurs and the chitin-protein microfibres are organised into macrofibres. ×21000

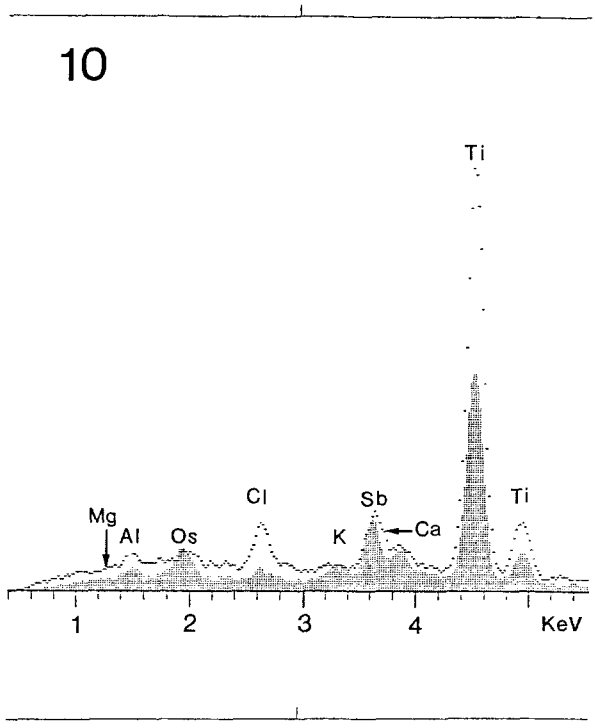

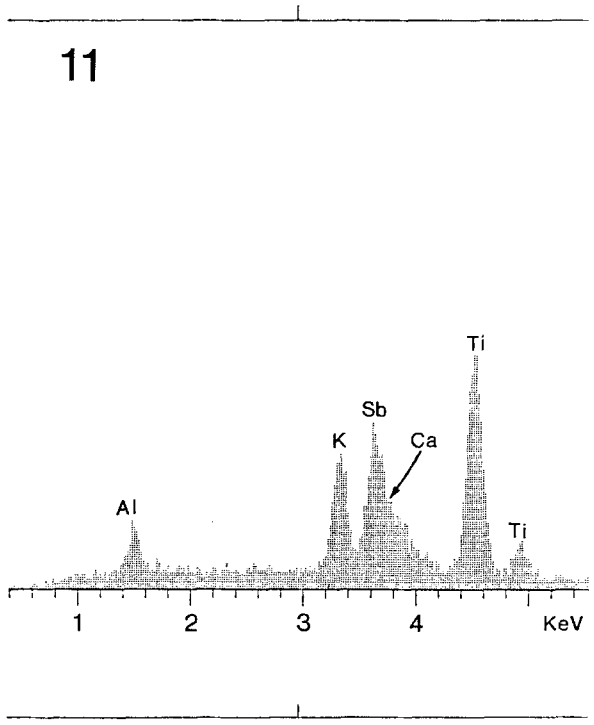

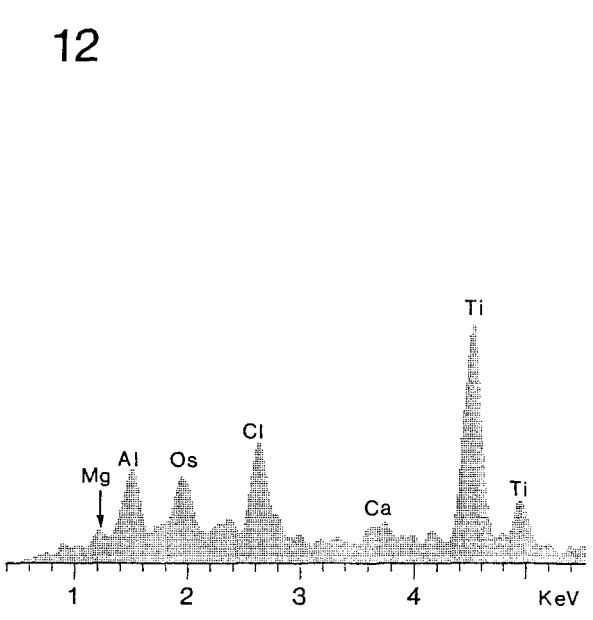

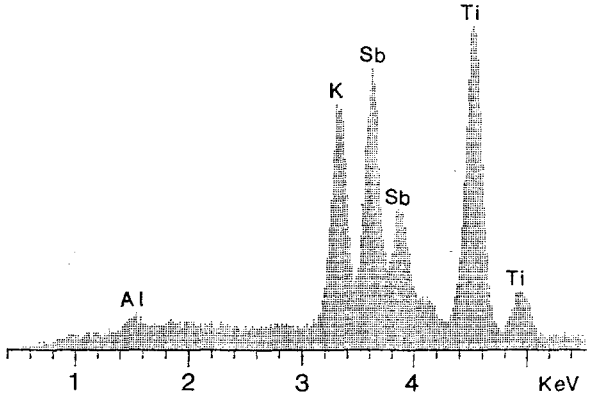

Figs. 10–13. X-ray microanalysis spectra of antimony precipitates. Aluminium ($K_{\alpha 1,2}$ at 1.486 keV) and titanium ($K_{\alpha 1,2}$ at 4.508 keV and $K_{\beta 1,3}$ at 4.931 keV) peaks correspond to the holder and the supporting gird, respectively

Fig. 10. Superimposition of spectra from the coarse precipitate particles (diameter > 100 nm) (*shadowed zone*) and the fine precipitate particles (diameter < 100 nm) (*dotted line*)

Fig. 11. Microdroplets of a $Ca(NO_3)_2/2Sb_2O_3$ + 4KOH standard solution in which the Sb/Ca ratio is 4

Fig. 12. Fine precipitate after stripping of the Sb peaks ($L_{\alpha 1}$, $L_{\beta 1}$ and $L_{\beta 2}$)

Fig. 13. Microdroplets of a $KSb(OH)_6$ standard solution

did not interfere with Ca peaks. Stripping of Sb peaks from the spectra revealed a small Ca peak at 3.690 keV in the fine precipitate only (Fig. 12). The coarse precipitate seemed to be Ca-free.

X-ray spectra from the subepicuticular region, the interprismatic septa (Fig. 14) and the prismatic spaces (Fig. 15) of the cuticle of premoulting crabs were obtained from freeze-sectioned and freeze-substituted fragments. They showed Ca peaks of similar magnitude to those obtained from the fine precipitate. An additional, an Mg peak ($K_{\alpha 1,2}$ at 1.253 keV) was clearly revealed on spectra from the subepicuticular region and the interprismatic septa (Fig. 14).

Concerning the mineral deposits, microanalysis of the pigmented (Fig. 16) and principal layers (Fig. 17) provided spectra with major Ca $K_{\alpha 1,2}$ and $K_{\beta 1,3}$ peaks (at

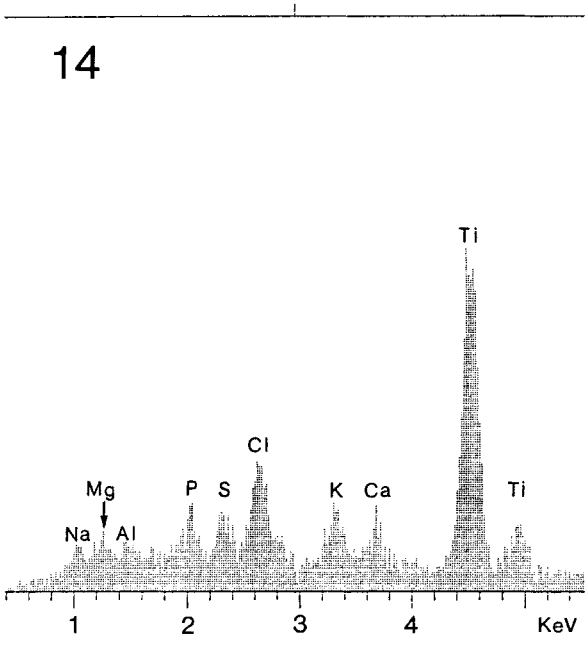

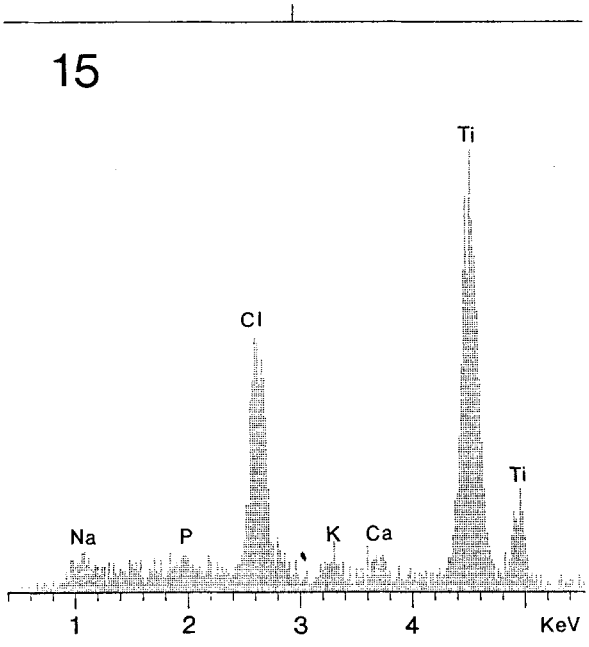

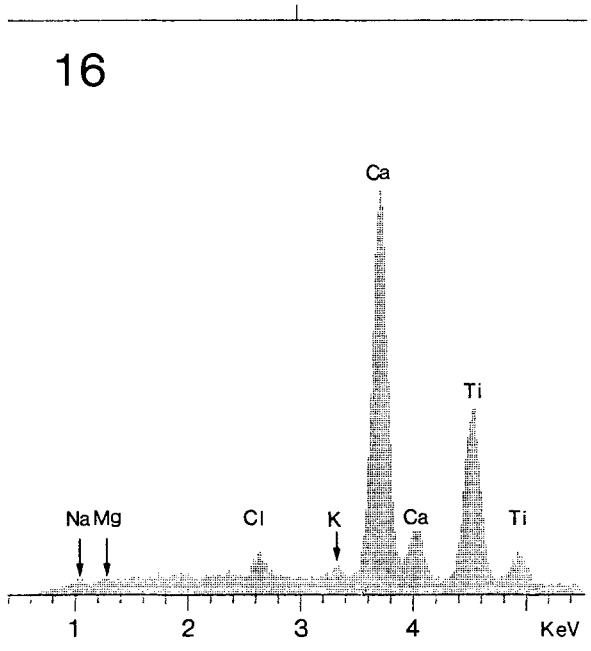

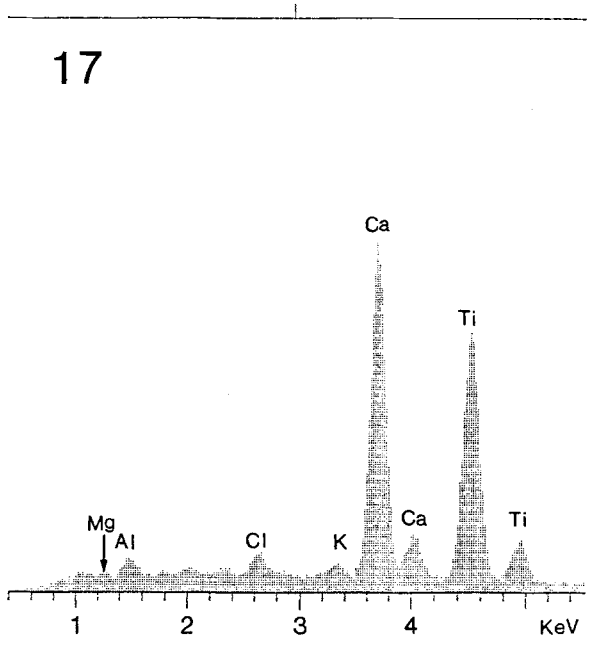

Figs. 14–17. X-ray microanalysis spectra of thin sections

Fig. 14. Subepicuticular region in a freeze-substituted sample of the late premoult cuticle

Fig. 15. Prismatic spaces of the pigmented layer in a thin frozen section of a cuticular fragment at stage D_2

Fig. 16. Mineral concretions below the epicuticle 24 h after exuviation (freeze-substituted sample)

Fig. 17. Mineral deposits in the principal layer 24 h after exuviation (freeze-substituted sample)

3.690 keV and 4,012 keV, respectively) and a significant Mg peak ($K_{\alpha 1,2}$ at 1.253 keV) in the pigmented layer (Fig. 16).

Discussion

The K-pyroantimonate technique was originally intended for locating Na at the ultrastructural level (Komnick 1962). Pyroantimonate was later used successfully as a cytochemical marker of ionic Ca in a wide variety of tissues (Spicer et al. 1969; Saetersdal et al. 1974; Stoeckel et al. 1975; Weringer et al. 1978; Weakley 1979; van Iren et al. 1979; Morris and Appleton 1980; Wick and Hepler 1982; Meyran et al. 1984, 1986). The method requires careful controls and cautious interpretation because antimonate forms precipitates with several cations, namely Na^+, Ca^{2+}, Mg^{2+}, K^+ and H^+, and with organic cations

under appropriate conditions (Clark and Ackerman 1971; Klein et al. 1972; Tisher et al. 1972). Nevertheless, the various precipitates can be accurately identified on the basis of their sensitivity to water and EDTA, and by X-ray microanalysis (Wick and Hepler 1982). In the present investigation, these controls clearly indicate that Ca^{2+} and Mg^{2+} are the main components of the fine precipitate, whereas they are completely lacking in the coarse precipitate, which probably results from the precipitation of unrinsed $KSb(OH)_6$ during the alcoholic dehydration procedure (Tisher et al. 1972; Hayat 1975). The morphological appearance and particle size of the fine precipitate, including the particles lining the plasma membrane of the epidermal cell extensions, closely resemble those of the Ca-pyroantimonate deposits obtained in various tissues by several authors (Saetersdal et al. 1974; Simson and Spicer 1975; Meyran et al. 1984, 1986). On the basis of these results, we shall discuss the significance of the distribution of Ca and Mg in relation to their transport pathway through the cuticle during moulting and mineralisation.

Ca and Mg distributions related to mineral deposition

Since the observations of Drach (1937,1939), it has been acknowledged that cuticular mineralisation in *Carcinus maenas* begins between 4 and 10 h postmoult, with the deposition of the first Mg-calcite crystals. Our results further show that, during the premoult, Ca and Mg accumulate at specific sites in the pigmented layer. Despite the small peaks observed on X-ray spectra, the presence of substantial amounts of Mg is clearly revealed in quantitative analysis (Compère et al. 1992). In agreement with Drach (1937, 1939), Bouligand (1970) and Giraud-Guille and Quintana (1982), we have observed that these sites are preferentially mineralised shortly after moulting, i.e., in the first 24 h postmoult. Consequently, the mineralised interprismatic septa of the pigmented layer appear to be sandwiched between two horizontal mineralised layers (the outermost lamella below the epicuticle and the lowermost lamella associated with those of the principal layer), giving vertical walls. These form a honeycomb-like structure that quickly increases the rigidity of the new cuticle despite the small supply of newly recruited material. The double role of these special sites of the pigmented layer, namely the accumulation of divalent cations before moulting and preferential mineralisation after moulting (Giraud 1977; Giraud-Guille and Quintana 1982), is probably related to the presence of polyanionic glycoproteins rich in carboxylic mucopolysaccharides. These have been identified and located by Giraud (1977) and Guiraud-Guille (1984a). In relation to the hypothesis of Tandler et al. (1970) and Wick and Hepler (1982) concerning the availability of cations for pyroantimonate precipitation, this could mean that in the premoult cuticle, Ca and Mg are "loosely bound" to polyanionic macromolecules by electrostatic linkages, thus producing an abundant pyroantimonate precipitate. According to these authors, pyroantimonate precipitates only those ions that are "loosely bound" to macromolecular components, whereas freely diffusible ions are too rapidly washed out of the tissue and very tightly bound ions are largely unreactive.

The presence of mineral in the epicuticular layers is controversial. Our present observations combined with the ultrastructural description of the inner epicuticle (Compère and Goffinet 1987a) provide an explanation that may reconcile the apparently conflicting findings of the various authors. The heavy mineral deposit filling the spaces between the conical roots of the inner epicuticle is probably the same as that thought to be located in vertical epicuticular canals of 100–250 nm in diameter (Travis 1957; Neville 1975; Hegdahl et al. 1977c; Roer and Dillaman 1984). It has been demonstrated, however, that these spaces coincide with the upper ends of the procuticular pore canals. In crabs, these inter-radicular spaces extend only into the lower part of the inner epicuticle. On the other hand, the absence of mineral deposits in the upper part of this layer can explain the observations of Bouligand (1970) and Giraud-Guille (1984b), who consider the epicuticle of *Cancer pagurus* and *Carcinus maenas* to be unmineralised. In other species, such as the crayfish (Kümmel et al. 1970; Neville 1975), the interradicular spaces extend close to the cuticulin layer. When they are filled with mineral deposits, the whole epicuticular thickness thus appears mineralised. This could also explain the observation of Hegdahl et al. (1977c), who report the presence of mineral concretions in epicuticular spines of *Cancer pagurus*. Epicuticular spines contain an axial canal that is formed, as are the interradicular spaces, by a procuticular canal cell process at the early premoult stage (Compère, unpublished result). If the epicuticular layers are defined sensu stricto, as being the surface coat, the cuticulin layer and the matrix of the inner epicuticle (Compère 1988), we may conclude that these layers are not mineralised, in agreement with Drach (1937), Richards (1951), Hackman (1984), Bouligand (1970, 1988) and Giraud-Guille (1984b). The lack of mineral deposits in the epicuticular canals might be surprising, as they contain sufficient quantities of Ca and Mg ions to induce pyroantimonate precipitation. In reality, their diameter (25 nm) is probably too small to allow growth of calcite crystals, which require a minimal breadth of at least 30 nm (Bouligand 1988).

Role of the intracuticular pore canals in the mineralisation process

The experiments of Roer (1980), Cameron and Wood (1985) and Cameron (1989) have shown that the epidermis plays a major physiological role in the mineralisation of the crustacean cuticle. The present results strongly support the view that the transfer of Ca and Mg ions from the epidermis into the mineralising cuticular layers during postmoult mineralisation of the cuticle is effected exclusively by the epidermal cell extensions: in pyroantimonate-treated postmoult samples, the plasma membrane of these cell extensions is obviously labelled by a substantial Ca-pyroantimonate precipitate. The location of these particles on the cytoplasmic leaflet of the plasma

membrane, their size (30–60 nm) and their crescent-like shape are features shared by the Ca-pyroantimonate precipitates obtained in other tissues involved in the active transport of Ca^{2+} (Simson and Spicer 1975; Meyran et al. 1984). These precipitate particles probably mark the Ca-transporting sites (Ca^{2+} ATPase, Ca^{2+}/Na^{+} and/or Ca^{2+}/H^{+} exchange mechanisms) whose presence on the apical plasma membrane of the epidermal cells has been reported by Roer (1980) and Cameron (1989) in *Carcinus maenas* and *Callinectes sapidus*, respectively. Eisenmann et al. (1990) suggest that, in rat incisor ameloblasts, an identical association exists between the formation of Ca-pyroantimonate precipitate along the apical cell membrane and the location of the Ca^{2+}, Mg^{2+}-ATPase. Furthermore, fluoride, which inhibits enamel mineralisation, and verapamil, a Ca-channel blocker, have been found to reduce the concentration of Ca-pyroantimonate deposits on the cell membrane of ameloblasts (Monsour et al. 1989). In accordance with the hypothesis of Tandler et al. (1970) and Wick and Hepler (1982), one might propose that the presence of Ca and Mg cations "loosely bound" to the affinity sites of ATPase induces the precipitation of pyroantimonate. The absence of precipitate particles in the organisation zone of chitin-protein fibres and along the cell apical plasma membrane between the pore canal cell extensions suggests that these structures are not Ca- or Mg-transporting pathways.

By 24 h after moulting, the distribution of mineral deposits is such that the cell extensions running through the mineralised lamellae of the principal layer constitute the preferential access routes up to the pigmented layer where mineralisation is still in progress. At this level, the regression of the epidermal cell extensions observed by Compère and Goffinet (1987b) shortly precedes the centripetal progress of mineral deposition. The different sequence of events occurring in these cuticular layers explains why the lumina of pore canals of the pigmented layer in the intermoult cuticle are filled with mineral, as previously observed by Travis (1957, 1963, 1965), Travis and Friberg (1963) and Hegdahl et al. (1977b), whereas they remain free in the principal layer, as mentioned by Bouligand (1970), Hegdahl et al. (1977a), Giraud-Guille (1984a) and Compère and Goffinet (1987b). During the postmoult period, rapid degeneration of the cell processes in the principal layer coincides with the complete mineralisation of the pigmented layer at stage C_1, and with the end of their transporting activity at stage C_3, precisely at the onset of deposition of the unmineralised membranous layer.

The question remains regarding the site of storage of the Ca^{2+} and Mg^{2+} accumulating in the new pigmented layer before the moult. Roer's in vitro experiments (1980) on the integument of *Carcinus maenas* suggest that the epidermis, at this time, is involved in resorption of Ca from the old cuticle. This view is inconsistent with the results of Cameron and Wood (1985) and of Jeuniaux et al. (1986), who have demonstrated that, in *Callinectes sapidus* and in *Carcinus maenas* respectively, the exuvium is shed with its entire Ca content. It thus appears that the cations accumulating in the new pigmented layer do not come from the old cuticle. As in the principal layer during the postmoult period, a thin cuticular zone near the epidermis remains free of any Sb precipitate. This observation supports the view that Ca ions are likewise transported by way of the cell extensions. During the premoult, however, the Ca-transporting rate is probably too low to induce Sb precipitation at the level of Ca-transporting sites in the plasma membrane.

Acknowledgements. P.C. is grateful for the hospitality shown to him while a visitor at the University College Cardiff to carry out the X-ray microanalytical part of this work. The authors thank Mrs. C. Winters (X-ray microanalysis), Mrs. N. Decloux (ultramicrotomy) and Mrs. C. Breeur (photography) for their excellent technical guidance and assistance, and Mrs. O. Gilson for typing the manuscript. They are indebted to the Belgian Joint Basic Research Fund for its financial support of this work (FRFC, convention N°.2.4527.89). P.C. is a research assistant of the National Fund for the Scientific Research (F.N.R.S., Belgium).

References

Appleton J, Morris DC (1979) The use of the potassium pyroantimonate-osmium method as a means of identifying and localizing calcium at the ultrastructural level in the cell calcifying systems. J Histochem Cytochem 27:676–680

Bouligand Y (1965) Sur l'achitecture torsadée répandue dans de nombreuses cuticules d'Arthropodes. CR Acad Sci Paris 261:3665–3668

Bouligand Y (1970) Aspects ultrastructuraux de la calcification chez les crabes. 7me Congrès Int Microsc Elect (Grenoble) 3:105–106

Bouligand Y (1972) Twisted fibrous arrangements in biological materials and cholesteric mesophases. Tissue Cell 4:189-217

Bouligand Y (1988) Problèmes de morphogenèse cuticulaire chez les Crustacés. Act Coll IFREMER 8:13–32

Cameron JN (1985) La mue du crabe bleu. Pour Sci 105:16–23

Cameron JN (1989) Post-molt calcification in the blue crab *Callinectes sapidus*: timing and mechanism. J Exp Biol 143:285–304

Cameron JN, Wood CM (1985) Apparent H^{+} excretion and CO_2 dynamics accompanying carapace mineralization in the blue crab (*Callinectes sapidus*) following moulting. J Exp Biol 114:181–196

Clark NA, Ackerman GA (1971) A histochemical evaluation of the pyroantimonate osmium reaction. J Histochem Cytochem 19:727–737

Compère P (1988) Mise en place de l'épicuticule chez le crabe *Carcinus maenas*. Act Coll IFREMER 8:47-54

Compère P, Goffinet G (1987a) Ultrastructural shape and three-dimensional organization of the intracuticular canal systems in the mineralized cuticle of the green crab *Carcinus maenas*. Tissue Cell 19:839–857

Compère P, Goffinet G (1987b) Elaboration and ultrastructural changes of the pore canal system in the mineralized cuticle of *Carcinus maenas* during the molting cycle. Tissue Cell 19:859–875

Compère P, Goffinet G (1992) Organisation tridimensionnelle et cytochimie de l'épicuticule et des systèmes canaliculaires des sclérites du crabe *Carcinus maenas* (Crustacé Décapode). Mém. Soc R Belge Ent 35:715–720

Compère P, Morgan JA, Winters C, Goffinet G (1992) X-ray microanalytical and cytochemical study of the mineralization process in the shore crab cuticle. Micron Microsc Acta 23:355–356

Drach P (1937) Morphogenèse de la mosaïque cristalline externe dans le squelette tégumentaire des décapodes branchyoures. CR Acad Sci Paris 205:1173–1176

Drach P (1939) Mue et cycle d'intermue chez les Crustacés Décapodes. Ann Inst Océan 19:103–392

Drach P, Tchernigovtzeff C (1967) Sur la méthode de détermination des stades d'intermue et son application générale aux Crustacés. Vie Milieu [A] Biol Mar 18:595–609

Eisenmann DR, Salama AH, Zaki ME, Ashrafi SH (1990) Cytochemical localization of calcium and Ca^{2+}, Mg^{2+} adenosine triphosphatase in colchicine-altered rat incisor ameloblasts. J Histochem Cytochem 38:1469–1478

Giraud MM (1977) Histochimie des premières étapes de la minéralisation de la cuticule du crabe *Carcinus maenas*. CR Acad Sci Paris 284:1541–1544

Giraud-Guille MM (1984a) Calcification initiation sites in the crab cuticle: the interprismatic septa. An ultrastructural cytochemical study. Cell Tissue Res 236:413–420

Giraud-Guille MM (1984b) Les matrices extracellulaires analogues de cristaux liquides. Structure et biominéralisation. Exemple de la cuticule du crabe *Carcinus maenas*. Thèse de Doctorat d'Etat, Univ P & M Curie, Paris 6, p 206

Giraud-Guille MM, Quintana C (1982) Secondary ion microanalysis of the crab calcified cuticle: distribution of mineral elements and interaction with the cholesteric organic matrix. Biol Cell 44:57–68

Green JP, Neff MR (1972) A survey of the structures of the integument of the fiddler crab *Uca pugilator*. Tissue Cell 4:137–171

Hackman RH (1984) Arthropoda cuticle: biochemistry. In: Bereiter-Hahn H, Matoltsy AG, Richards KS (eds) Biology of the integument. I. Invertebrates. Springer, Berlin Heidelberg New York, pp 583–610

Hayat MA (1975) Positive staining for electron microscopy. Van Nostrand, New York Cincinnati Toronto, p 361

Hegdahl T, Silness J, Gustavsen F (1977a) The structure and mineralization of the carapace of the crab (*Cancer pagurus* L.). I. The endocuticle. Zool Scripta 6:89–99

Hegdahl T, Gustavsen F, Silness J (1977b) The structure and mineralization of the carapace of the crab (*Cancer pagurus* L.). II. The exocuticle. Zool Scripta 6:101–105

Hegdahl T, Gustavsen F, Silness J (1977c) The structure and mineralization of the carapace of the crab (*Cancer pagurus* L.). III. The epicuticle. Zool Scripta 6:215–220

Iren F van, Essen-Joolen L van, Duyn-Schouten P van der , Boers-van der Sluitz R, Bruijn WC de (1979) Sodium and calcium localization in cells and tissue by precipitation with antimonate: a quantitative study. Histochemistry 63:273–294

Jeuniaux C, Compère P, Goffinet G (1986) Structure, synthèse et dégradation des chitinoprotéines de la cuticule des Crustacés décapodes. Boll Zool 53:183–196

Klein RL, Yen SS, Thureson-Klein A (1972) Critique on K-pyroantimonate method for semiquantitative estimation of cations in conjunction with electron microscopy. J Histochem Cytochem 20:65–78

Komnick H (1962) Elektronenmikroskopische Lokalisation von Na^+ und Cl^- in Zellen und Geweben. Protoplasma 55:414–418

Kümmel F, Claassen H, Keller R (1970) Zur Feinstruktur von Cuticula und Epidermis beim Flusskrebs *Orconectes limosus* während eines Häutungszyklus. Z Zellforsch Mikrosk Anat 109:517–551

Mentré P, Escaig F, Halpern S (1986) Amélioration de la méthode au pyroantimonate pour la localisation du sodium et du calcium au niveau utrastructural. Biol Cell 57:31a

Meyran JC, Graf F, Nicaise G (1984) Calcium pathway through a mineralizing epithelium in the crustacean *Orchestia* in premolt; ultrastructural cytochemistry and X-ray microanalysis. Tissue Cell 16:269–286

Meyran JC, Graf F, Nicaise G (1986) Pulse discharge of calcium through a demineralizing epithelium in the crustacean *Orchestia*: ultrastructural cytochemistry and X-ray microanalysis. Tissue Cell 18:267–283

Monsour PA, Douglas JH, Warshawsky H (1989) Effects of acute doses of sodium fluoride on the morphology and the detectable calcium associated with secretory ameloblasts in rat incisors. J Histochem Cytochem 37:463–471

Morgan AJ, Davies TW (1982) An electron microprobe study of the influence of beam current density on the stability of detectable elements in mineral salts (isoatomic) microdroplets. J Microsc 125:103–116

Morgan AJ, Davies TW, Erasmus DA (1975) Analysis of droplets from isoatomic solutions as a means of calibrating a transmission electron analytical microscope (TEAM). J Microsc 104:271–280

Morris DC, Appleton J (1980) Ultrastructural localization of calcium in the mandibular condylar growth cartilage of the rat. Calcif Tissue Int 30:27–34

Neville AC (1975) Calcification. In: Hoar WS, Jacobs J, Langer H, Lindauer M (eds) Zoophysiology and ecology, vol 4/5. Biology of the arthropod cuticle. Springer, Berlin Heidelberg New York, pp 307–318

Reynolds ES (1963) The use of lead citrate at high pH as an electron opaque stain in EM. J Cell Biol 17:208–211

Richards AG (1951) The integument of Arthropods. University of Minnesota Press, Minneapolis, p 411

Roer RD (1980) Mechanisms of resorption and deposition of calcium in the carapace of the crab *Carcinus maenas*. Exp Biol 88:205-218

Roer RD, Dillaman R (1984) The structure and calcification of the crustacean cuticle. Am Zool 24:892–909

Saetersdal TS, Myklebust R, Bergjustejen NP, Olsen WC (1974) Ultrastructural localization of calcium in the pigeon papillary muscle as demonstrated by cytochemical studies and X-ray microanalysis. Cell Tissue Res 155:57–74

Simson JAV, Spicer SS (1975) Selective subcellular localization of cations with variants of the potassium (pyro)antimonate technique. J Histochem Cytochem 23:575–598

Spicer SS, Greene WB, Hardin JH (1969) Ultrastructural localization of acid mucosubstances and antimonate-precipitable cation in human and rabbit platelets and megakaryocytes. J Histochem Cytochem 17:781–792

Stoeckel ME, Hindelang-Gertner C, Dillmann HD, Porte A, Stutinsky F (1975) Subcellular localization of calcium in the mouse hypophysis. I. Calcium distribution in adeno- and neurohypophysis under normal conditions. Cell Tissue Res 157:307–392

Tandler CJ, Libanati CM, Sanchis CA (1970) The intracellular localization of inorganic cations with potassium pyroantimonate. Electron microscope and microprobe analysis. J Cell Biol 45:355–367

Tisher CC, Weavers BA, Cirksena WJ (1972) X-ray microanalysis of pyroantimonate complexes in rat kidney. Am J Pathol 79:255–261

Travis DF (1957) The moulting cycle in the spiny lobster, *Palinurus argus* Latreille. IV. Post-ecdysial histological and histochemical changes in the hepatopancreas and integumental tissues. Biol Bull 113:451–457

Travis DF (1963) Structural features of mineralization from tissue to macromolecular levels of organization in the decapod Crustacean. Ann NY Acad Sci 109:117-245

Travis DF (1965) The deposition of skeletal structures in Crustacea. V. The histomorphological and histochemical changes associated with the development and calcification of branchial exoskeleton in the crayfish, *Orconectes virilis* Hagen. Acta Histochem 20:193–222

Travis DF, Friberg U (1963) The deposition of skeletal structures in Crustacea. VI. Microradiographic studies of the exoskeleton of the crayfish *Orconectes virilis* Hagen. J Ultrastruct Res 9:285-301

Vigh DA, Dendinger J (1982) Temporal relationship of postmolt deposition of calcium, magnesium, chitin and protein in the cuticle of the Atlantic blue crab *Callinectes sapidus* Rathbum. Comp Biochem Physiol [A] 72:365–369

Vitzou AM (1882) Recherches sur la structure et la formation des téguments chez les Crustacés Décapodes. Arch Zool Exp 10:451–476

Watson ML (1958) Staining of tissue sections for electron microscopy with heavy metals. J Biophys Biochem Cytol 4:475–478

Weakley BS (1979) A variant of the pyroantimonate technique suitable for localization of calcium in ovarian tissue. J Histochem Cytochem 27:1017-1028

Welinder BS (1975) The crustacean cuticle. II. Deposition of organic and inorganic material in the cuticle of *Astacus fluviatilis* in the period after molting. Comp Biochem Physiol [B] 51:409–416

Weringer EJ, Oldham SB, Bethune JE (1978) A proposed cellular mechanism for calcium transport in the intestinal epithelial cell. Calc Tissue Res 26:71–79

Wick SM, Hepler, PD (1982) Selective localization of intracellular Ca with potassium pyroantimonate. J Histochem Cytochem 30:1190–1204

Yano I (1980) Calcification of crab cuticle. In: Omori M, Watabe N (eds) The mechanisms of biomineralization in animals and plants. Proc 3rd Int Biomineralization Symp, Tokai University Press, pp 187–196